AJNR

Three-dimensional phase-contrast MR angiography in the head and neck: preliminary report.

J R Pernicone, J E Siebert, E J Potchen, A Pera, C L Dumoulin and S P Souza

AJNR Am J Neuroradiol 1990, 11 (3) 457-466
http://www.ajnr.org/content/11/3/457

Three-Dimensional Phase-Contrast MR Angiography in the Head and Neck: Preliminary Report

Joseph R. Pernicone[1]
James E. Siebert[1]
E. James Potchen[1]
Abraham Pera[2]
Charles L. Dumoulin[3]
Steven P. Souza[3]

Morbidity and possible mortality associated with contrast angiography lead to its cautious use. A noninvasive method for screening and further delineating known abnormalities would be welcomed. This article reviews the initial results and application of MR imaging to vascular imaging in the head and neck. By using the three-dimensional phase-sensitive method of Dumoulin, Souza, and collaborators, we acquired MR angiograms in 37 min and portrayed blood flow in all the major arteries and veins. Feeding arteries and draining veins of arteriovenous malformations were well delineated; aneurysms as small as 3–4 mm were shown, and obstructed cerebral vessels and the patency of a highly stenotic internal carotid artery were demonstrated.

MR angiography of the head or neck offers great promise as a noninvasive means of studying vascular abnormalities.

***AJNR* 11:457–466, May/June 1990; *AJR* 155: July 1990**

Contrast angiography is a reliable method for obtaining morphologic, and to some extent, hemodynamic information about blood vessels. Morbidity associated with angiographic procedures, however, includes the possibility of stroke, renal failure, and patient discomfort from catheter insertion and contrast injection [1]. A noninvasive alternative would be clearly desirable. This article discusses and gives examples of our initial experience with a phase-sensitive method of MR angiography [2–5], a totally noninvasive procedure. Our efforts have been directed toward continued development of the technique and the determination of clinical protocols in preparation for future prospective clinical studies.

Materials and Methods

Data are acquired by using a three-dimensional (3D) gradient-refocused spin-warp scan technique (General Electric 1.5-T MR imager, Version 3.2.C) that incorporates bipolar magnetic gradient pulses for phase-sensitive flow encoding [3]. Figure 1 depicts the RF and magnetic gradient pulse sequence used. The repetition time (TR) was 22.3 msec, the echo time (TE) was 14.7 msec, and the RF flip angle ranged from 15° to 30°. The number of excitations (NEX) per phase-encoding step was two. Flow-encoding gradient-pulse lobes were half-period sine functions of typically 3-msec duration with a peak value of 9.0 mT/m.

Before the MR study, the referring clinician is consulted to define the anatomic extent of interest to determine the minimum appropriate field of view (FOV) to be imaged. Table 1 presents frequently used selections for acquisition matrix and FOVs. All options listed have the same number of phase-encoding steps and, hence, the same acquisition times. The options are listed in order of decreasing acquisition voxel (effective volume element) size, the smallest voxel size being $(0.78\ mm)^3$.

Since currently only one flow direction can be encoded in an acquisition, three sequential acquisitions were performed for total flow information. The scanning time was approximately 12 min for each of the three directions of flow encoding. Hence, the total scan time was approximately 37 min. The three single-flow component volume images were then combined by vector addition to form a total-flow magnitude image.

Received March 14, 1989; revision requested May 12, 1989; revision received October 17, 1989; accepted November 2, 1989.

[1] Department of Radiology, Michigan State University, B220 Clinical Center, East Lansing, MI 48824. Address reprint requests to J. R. Pernicone.

[2] Hemet Valley Imaging Medical Group, Inc., P. O. Box 3897, Hemet, CA 92343.

[3] General Electric Company, Corporate Research and Development, P. O. Box 8, Schenectady, NY 12301.

0195–6108/90/1103–0457

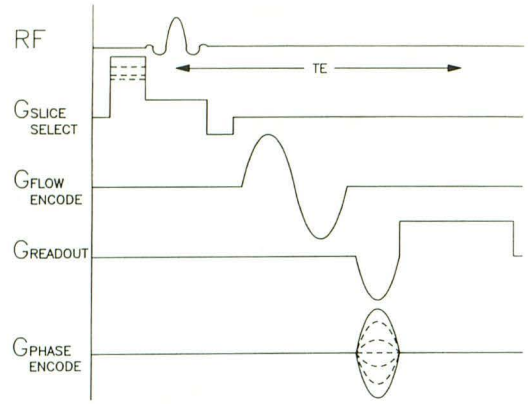

Fig. 1.—3D phase-contrast pulse sequence consisting of spoiled gradient-refocused sequence incorporating bipolar flow-encoding pulses. Two gradient directions of phase encoding are used. Flow-encoding pulses are placed on a single gradient direction during each of the three required 3D acquisitions. G = gradient.

TABLE 1: Acquisition Matrix and Field-of-View Selections in MR Phase-Contrast Angiography

Acquisition Matrix	Field of View (cm)	Voxel Dimensions (mm)[a]
256 × 128 × 128	24 × 24 × 24	0.94 × 1.88 × 1.88
	20 × 20 × 20	0.78 × 1.56 × 1.56
	20 × 20 × 10	0.78 × 1.56 × 0.78
256 × 256 × 64	20 × 20 × 5	0.78 × 0.78 × 0.78

Note.—Dimensions are given in an x × y × z sequence.
[a] Nonselective excitation can be used with head-coil reception.

Projection images were computed from the 3D MR angiogram image by selecting the maximum voxel intensity value along the projection ray path as the projection-image pixel (picture element of a two-dimensional [2D] digital image) value [6]. The projection images can be viewed singly or in cine format as a series of projections from progressive view angles about an axis of rotation to impart a 3D perspective. Also, projection images were computed over selected subvolumes (slabs) in axial, coronal, or sagittal orientations. Such primary axis projections we refer to as "collapse" images (seemingly collapsing a stack of slices).

Results

Several cases are described to demonstrate the clinical potential of phase-contrast MR angiography. We have performed over 90 studies in symptomatic and asymptomatic patients 13–91 years old, as well as numerous preliminary studies in control subjects.

A normal 30-year-old man appears in Figure 2. The 2D projection images (Figs. 2A–2C) are computed at 0°, 30°, and 60°, respectively, relative to the anteroposterior plane. They were selected from a larger set of 32 maximum pixel projections computed from the full 3D data set (24 × 24 × 24 cm FOV, 256 × 128 × 128 matrix, NEX = 2, 37-min scan time). All the major arteries (e.g., carotids, cerebral, and communicating) and veins are clearly delineated, as are most of the primary and secondary ramifications of these vessels. These few selected projections do not effectively convey the full anatomic detail present in the 3D data. When such projections at small incremental angles are viewed sequentially as a movie loop on a graphics console, many more vessels as well as the true 3D geometry of the vasculature are perceived.

Results of three studies in patient with cerebral aneurysms appear in Figures 3–5. The signal void from a 9-mm aneurysm is shown on an axial spin-echo image, 2000/80 (TR/TE), in a 45-year-old woman (Fig. 3A). Figures 3B–3D show that the void on spin echo represents flow in a 9-mm internal carotid artery bifurcation aneurysm. By interactively viewing the volume angiogram in multiple-projection views (one view shown in Fig. 3C), individual slices of the 3D image data (Fig. 3D), or collapse images (Fig. 3B), the connection of the aneurysm to the vessel from which it originates can be demonstrated. The neck of the aneurysm is seen clearly in the individual axial slice (Fig. 3D) of the 3D flow image. For comparison, Figures 3E and 3F are the lateral and anteroposterior contrast angiograms after common carotid injection.

Figure 4, the MR angiogram and contrast angiogram of a 65-year-old man, shows bilateral infundibula of the superior cerebellar arteries. In this acquisition, the FOV was limited to a region about the circle of Willis by exciting only a 5-cm slab (last entry, Table 1). Figure 4A is a projection through the 3D MR flow image angled to give a clear presentation of the infundibula. Figure 4B is the projection image of Figure 4A with the gray-scale mapping simply inverted. Inverting the gray-scale mapping mimics the appearance of subtraction contrast angiograms. Figure 4C is a computed magnification of a coronal collapse across the region of interest. On the right side, a 3- to 4-mm aneurysmal dilatation of the infundibulum is present, as evidenced by the size of the infundibulum and the suggestion that the distal portion of the vessel emerges eccentrically from the infundibulum. Figure 4D is a projection in the axial direction through the circle of Willis. The contrast angiogram after left vertebral artery injection (Fig. 4E) shows that the basilar artery feeds only the left posterior cerebral artery. Injection of the right carotid artery (not shown) indicated that the right posterior cerebral artery originated from the right posterior communicating artery. Note that the MR angiogram provided this information with one data acquisition (Fig. 4D).

A third example of aneurysm is illustrated in Figure 5. The anteroposterior MR angiogram projection image (Fig. 5A) shows a small right middle cerebral artery aneurysm. The acquisition method used a 10-cm excitation slab, demonstrating again the tradeoff between anatomic extent and spatial resolution. Figure 5B is an axial collapse image spanning the pertinent segment of the middle cerebral artery. Figure 5C is the anteroposterior contrast angiogram taken after right carotid injection. Both studies demonstrate similar characteristics as to the orientation, size, and shape of the aneurysm.

Arteriovenous malformations (AVMs) are well delineated by the phase-contrast method since both venous and arterial flow are imaged irrespective of vessel geometries. Figure 6 is from a 19-year-old woman with a large left-frontal-lobe AVM. The conventional T2-weighted axial spin-echo image (2000/

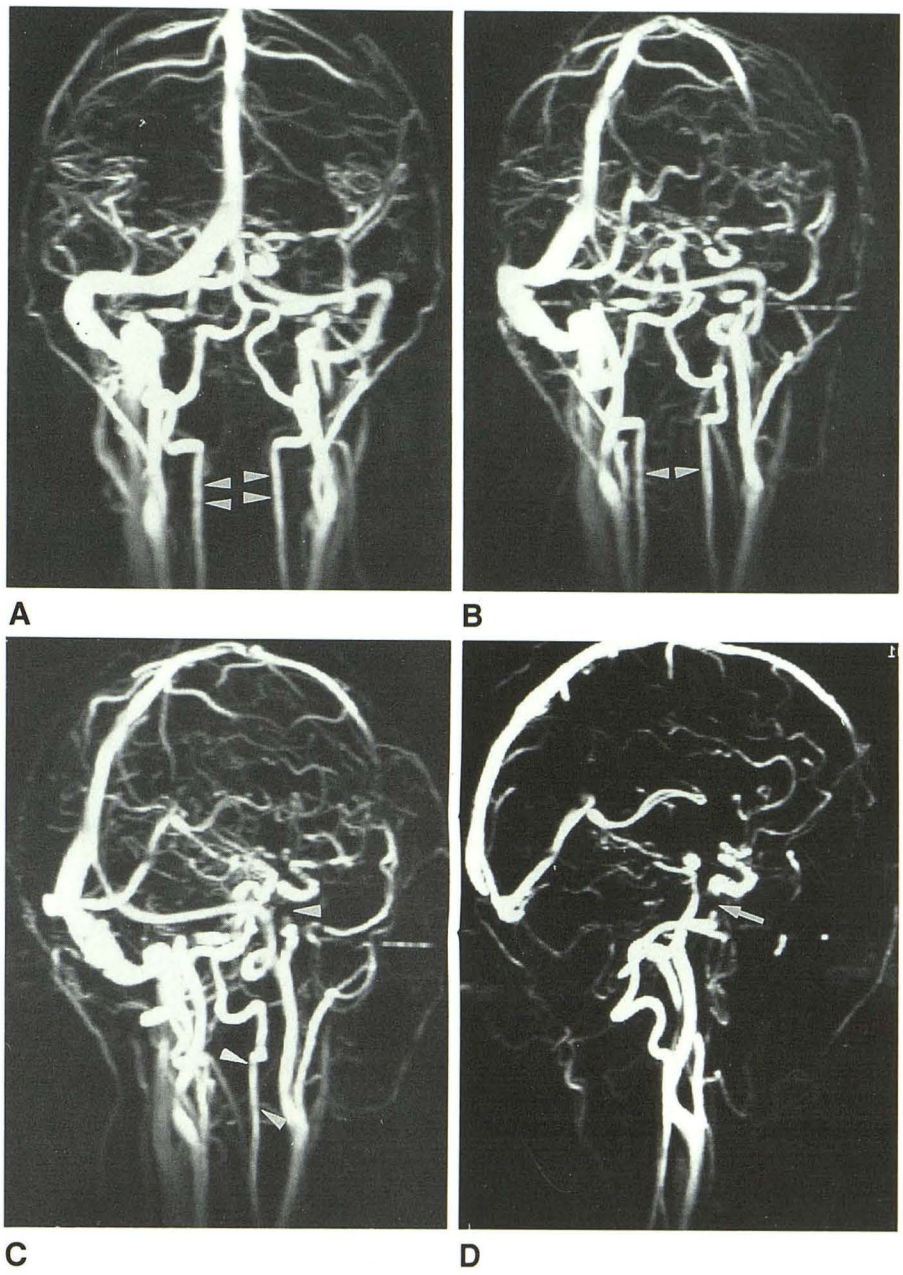

Fig. 2.—MR angiograms of 30-year-old normal male volunteer.

***A–C*, Maximum-intensity projection images computed from 3D flow image data at 0° (anteroposterior direction), 30°, and 60°, respectively.**

***D*, Projection through subset of sagittal slices (collapse image) spanning left hemisphere only.**

3D perspective is visualized when such projections are shown in movie loop format. Signal loss in the petrous portion of the internal carotid and vertebral arteries as they pass through transverse foramina is due to diamagnetic effects of bone (*arrowheads, arrow*).

80) through the AVM is shown in Figure 6A. MR angiograms appear in Figures 6B–6E. The large-FOV anteroposterior projection MR angiogram image (Fig. 6B) and lateral projection image (Fig. 6C) depict the extent of the AVM and all pertinent arteries and veins. Vessels around an AVM that are not directly related to it can be excluded from computed projection views by specifying a volume of interest enclosing the desired structures or by collapsing a subset of slices. By this method the feeding arteries and draining veins are shown more clearly. The coronal collapse image (Fig. 6D) and the axial collapse image (Fig. 6E) help to determine supply/return paths of the AVM. However, in this patient, early draining veins are not defined, as can be ascertained on contrast angiography (Figs. 6F and 6G).

Within the neck, the carotid and vertebral arteries and the jugular veins are well demonstrated on MR imaging. Even small amounts of flow beyond a very severe stenosis can be delineated (Figs. 7A and 7B). Visualization is enhanced by selecting a volume of interest that excludes most of the overlapping vessels (Fig. 7A). The corresponding contrast angiograms (Figs. 7C and 7D) demonstrated over 90% stenosis in the right internal carotid artery at its origin. The minute amount of flow past this stenosis is demonstrated by MR angiography.

Figure 8 is the phase-contrast MR angiogram of a 47-year-old man whose history was consistent with superior sagittal sinus thrombosis. This angiogram confirms the clinical impression by showing a lack of flow in the superior sagittal sinus.

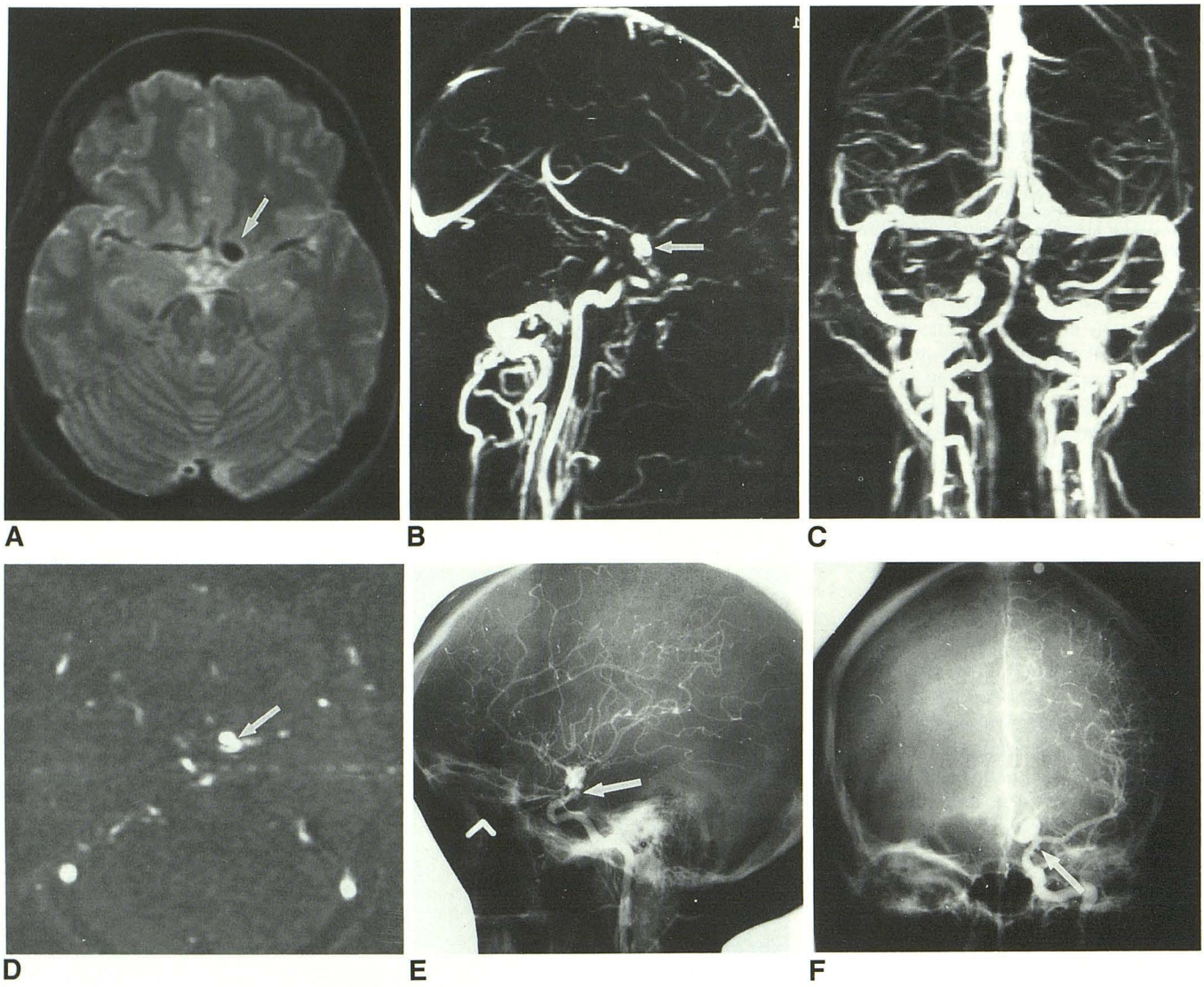

Fig. 3.—Aneurysm measuring 9 mm at bifurcation of internal carotid artery.
A, Spin-echo image (2000/80) through aneurysm (*arrow*).
B, Projection through subset of phase-contrast sagittal slices spanning aneurysm region (*arrow*).
C, Anteroposterior projection image through entire head.
D, Single axial slice shows neck of aneurysm (*arrow*).
E and *F*, Lateral (*E*) and anteroposterior (*F*) contrast angiograms after common carotid injection. Two additional small projections from carotid artery, which could represent aneurysms are seen best on anteroposterior angiogram (*arrows*) and were not demonstrated on MR angiogram. This is most likely due to slow flow and subsequent low signal in aneurysm, along with insufficient resolution owing to large acquired voxel size (0.9 × 1.9 × 1.9 mm).

In addition, it is noted that there is little or no flow in the transverse and sigmoid sinuses, or in the jugular veins bilaterally. Also, lack of flow in the left internal carotid artery is demonstrated.

Discussion

Flow Image Acquisition

The method of phase-contrast angiography uses a pulse sequence and subtraction technique such that the stationary tissue ideally contributes no signal to a voxel, whereas moving tissue contributes a signal related to its flow velocity. This is achieved with the use of bipolar flow-encoding gradient pulses, as depicted in Figure 9. A bipolar gradient pulse causes a phase shift, ϕ_1, proportional to motion given by $\phi_1 = \gamma\ VTA_g$, where γ is the gyromagnetic ratio, V the velocity of flow, T is the time separation of the center of the bipolar lobes, and A_g is the area under one lobe [2]. In the phase-contrast pulse sequence, the polarity of the bipolar gradient is inverted on alternate acquisitions (odd/even) for each phase-encoding step. An inverted bipolar pulse induces a phase shift, $\phi_2 = -\gamma VTA_g = -\phi_1$. Each flow image voxel is assigned a signal intensity proportional to the vector differ-

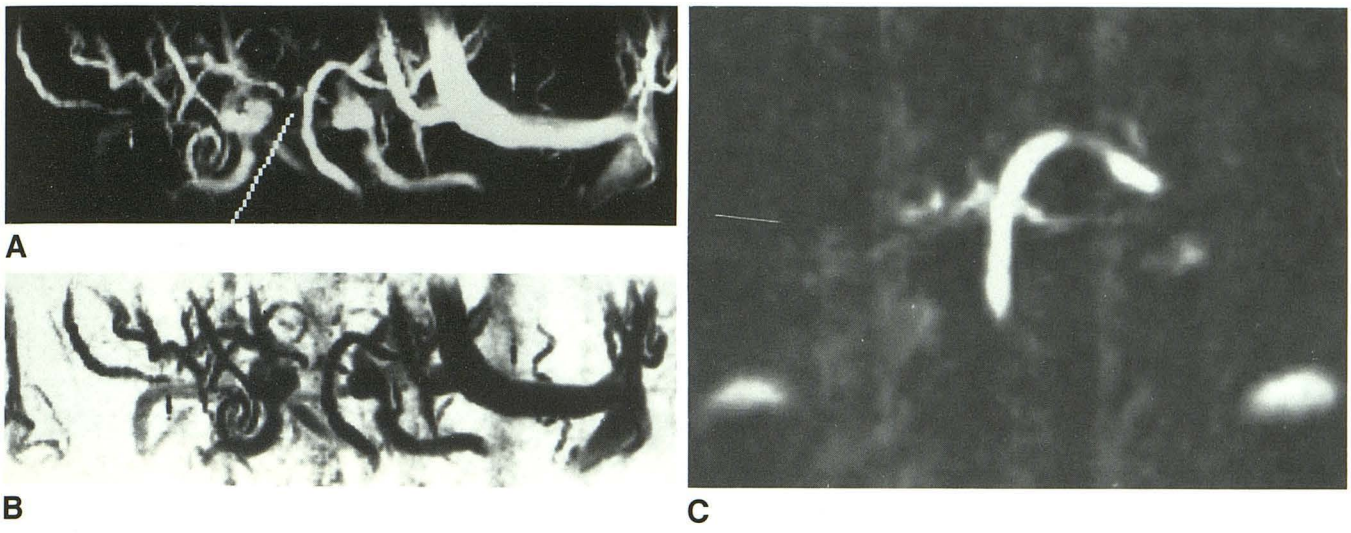

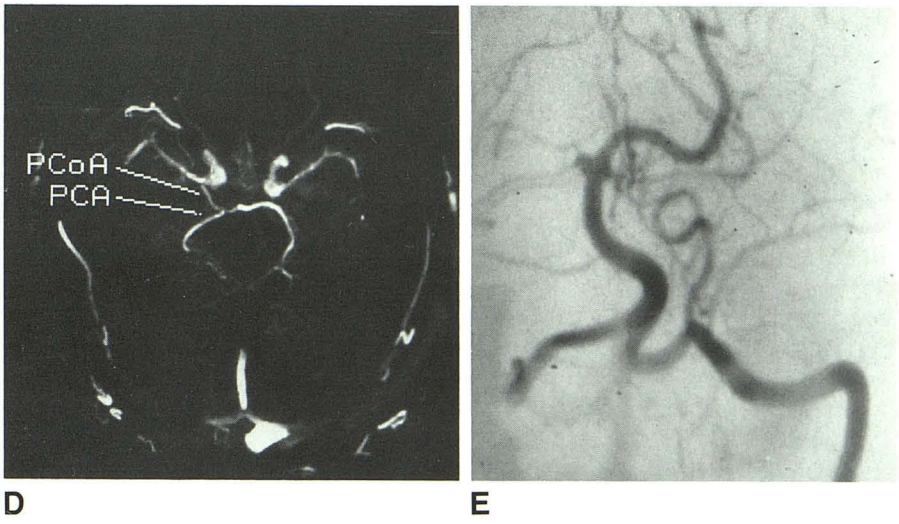

Fig. 4.—Bilateral infundibula of superior cerebellar arteries. Acquisition consisted of cubic voxels with 0.78-mm edges.

A, Projection image through entire data set angled to give clear presentation of infundibula.

B, Same projection image, but with the gray-scale mapping inverted to mimic subtraction contrast angiogram.

C, Magnified collapse image in coronal direction of infundibula at narrow window width setting. Note aneurysmal dilatation of right infundibulum.

D, Collapse image of axial slices of region of circle of Willis. PCoA = posterior communicating artery; PCA = posterior cerebral artery.

E, Contrast angiogram after left vertebral artery injection.

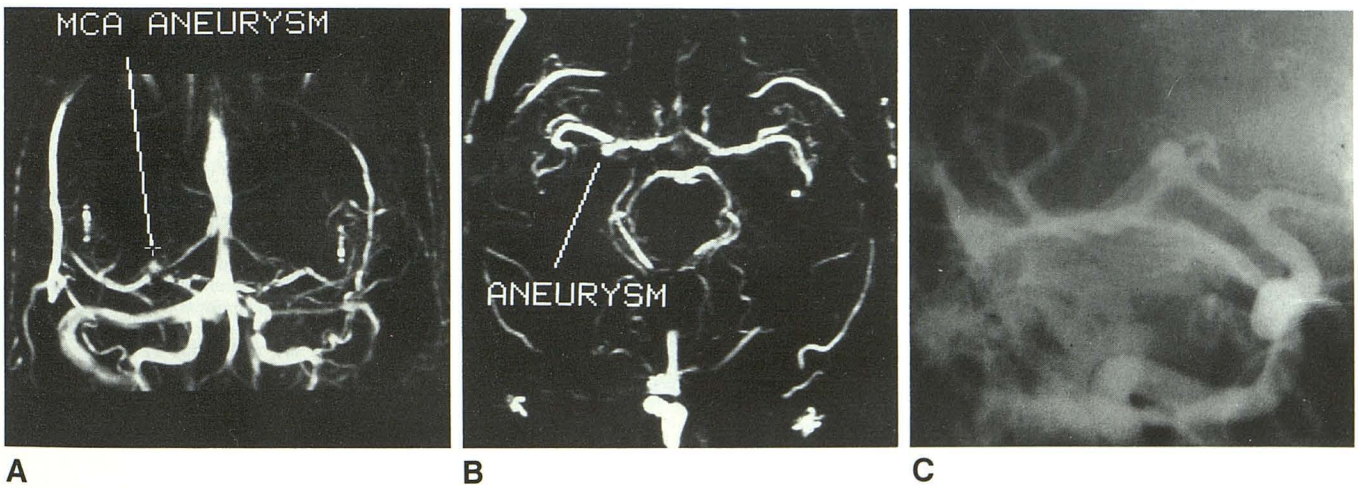

Fig. 5.—Aneurysm of right middle cerebral artery.

A, Anteroposterior projection image through entire volume image. Diminished signal in middle cerebral artery (MCA) at origin of aneurysm is explained by complex flow patterns.

B, Collapse image of axial slices containing relevant length of middle cerebral artery shows relationship of aneurysm and neck to parent vessel.

C, Anteroposterior contrast angiogram after right carotid injection.

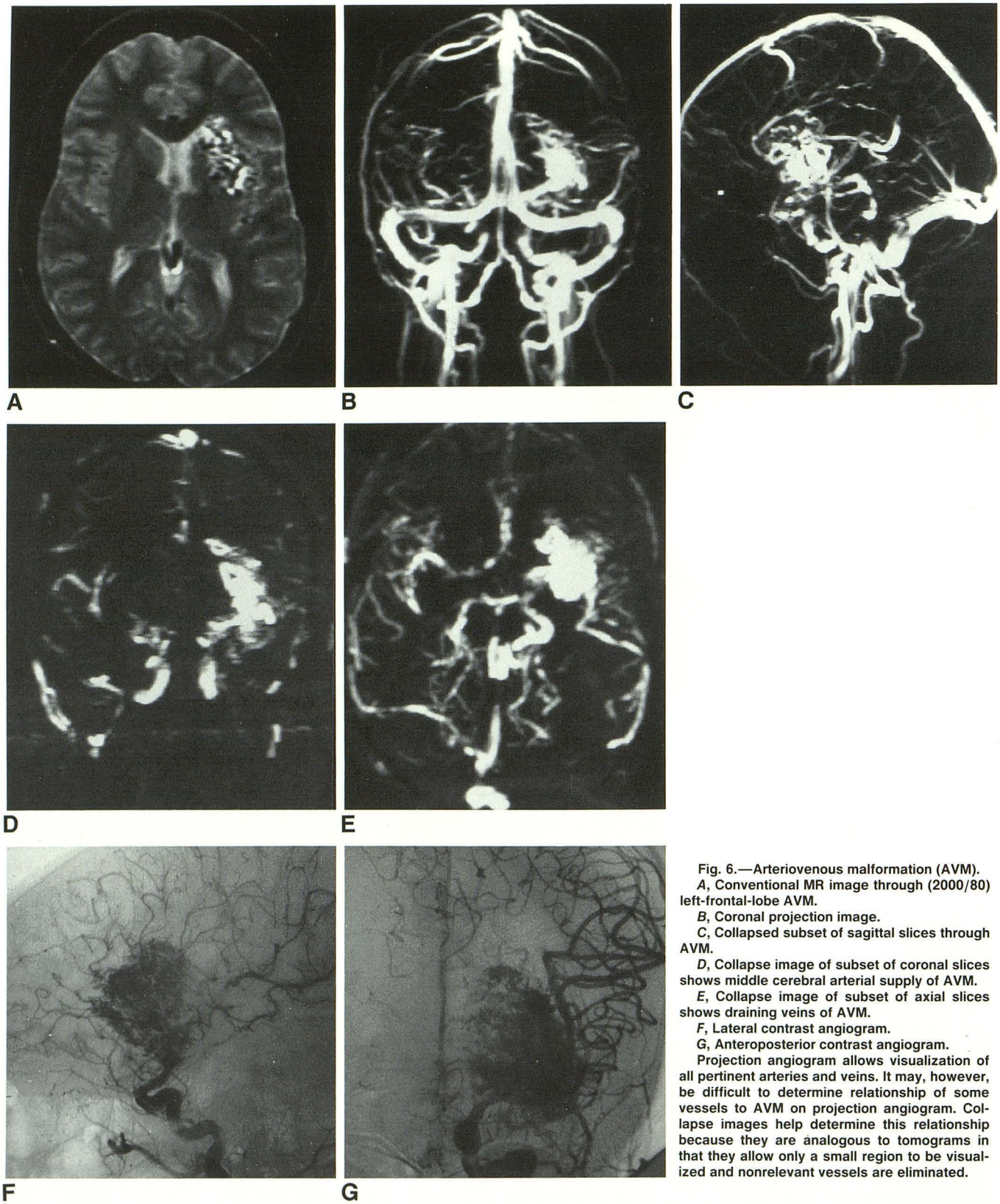

Fig. 6.—Arteriovenous malformation (AVM).
A, Conventional MR image through (2000/80) left-frontal-lobe AVM.
B, Coronal projection image.
C, Collapsed subset of sagittal slices through AVM.
D, Collapse image of subset of coronal slices shows middle cerebral arterial supply of AVM.
E, Collapse image of subset of axial slices shows draining veins of AVM.
F, Lateral contrast angiogram.
G, Anteroposterior contrast angiogram.
Projection angiogram allows visualization of all pertinent arteries and veins. It may, however, be difficult to determine relationship of some vessels to AVM on projection angiogram. Collapse images help determine this relationship because they are analogous to tomograms in that they allow only a small region to be visualized and nonrelevant vessels are eliminated.

ence in average transverse magnetization of the two above acquisitions. Since both bipolar pulse polarities cause zero phase shift for stationary tissue, nonzero contribution is made to voxel intensity only from moving spins.

The resulting contribution to voxel values in the magnitude image from each moving spin is proportional to $|\sin \phi_1|$. As a consequence of the properties of the sine function, the intensity contribution for moving tissue will increase until

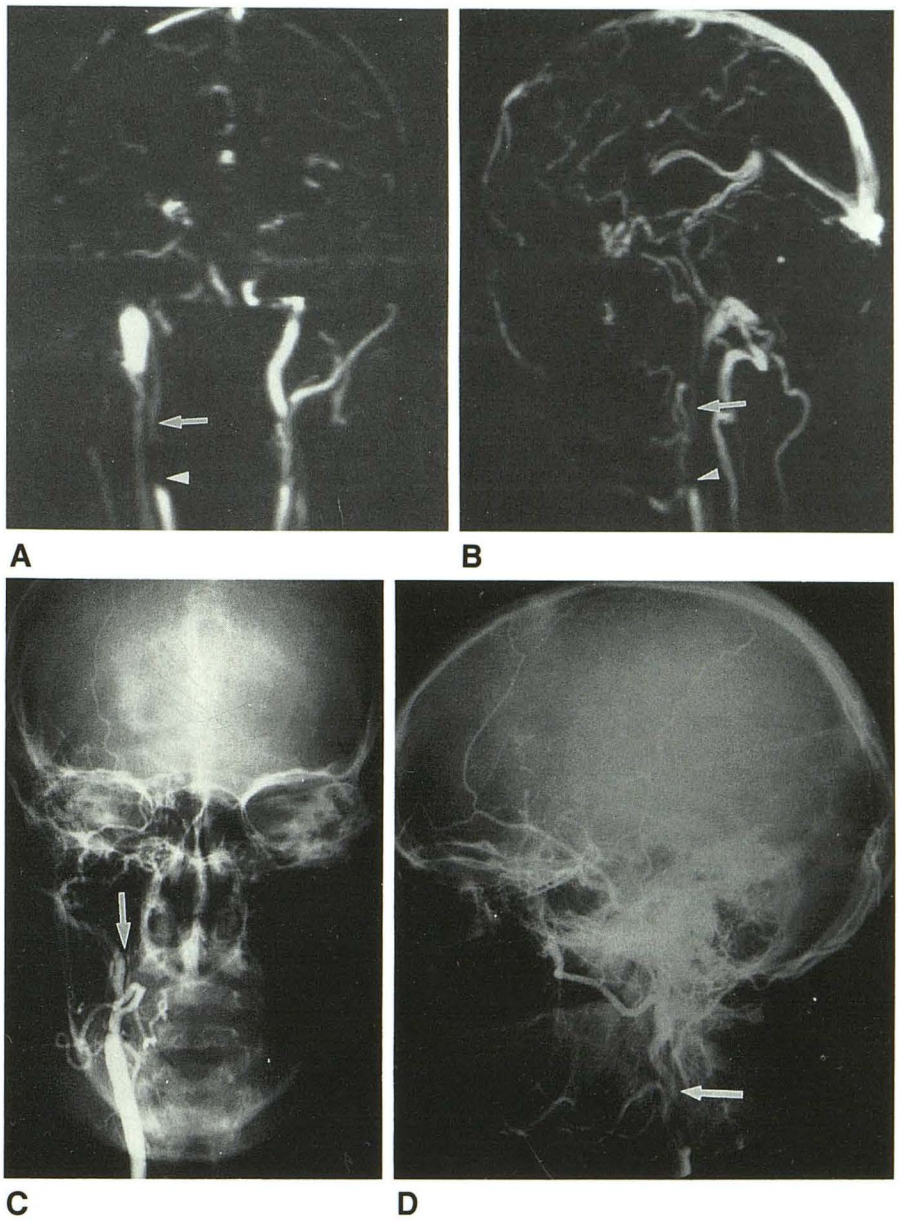

Fig. 7.—Carotid stenosis.

***A*, Collapse image of subset of coronal slices through internal carotid arteries.**

***B*, Collapse image of subset of sagittal slices through right internal carotid artery.**

***C* and *D*, Anteroposterior (*C*) and lateral (*D*) contrast angiograms after right common carotid injection.**

Disease is noted bilaterally but is more severe on right compared with left side. Internal carotid arteries (*arrows*). Signal is lost in proximal right internal carotid artery (*arrowhead*) owing to complex patterns of flow in poststenotic segment, but is regained more distally when laminar flow is reestablished. Since flow is seen proximal to first branch of right internal carotid artery, flow through stenotic segment at internal carotid artery origin is implied.

$\phi_1 = \pi/2$, which will give a maximum signal intensity. For larger values of ϕ_1, signal intensity will decrease to a value of zero when $\phi_1 = \pi$. Ideally, the parameters T and A_g are small enough so that sin $\phi_1 \approx \phi_1$ and, therefore, the voxel values approximate a linear function of flow velocity over the range of interest.

In clinical application, small vessels and wall details can be enhanced by using a higher degree of flow encoding. However, artifacts can arise from any resulting ambiguous flow encoding (more than one velocity mapping to a voxel value). To ensure that the flow-image voxel values increase monotonically with flow velocity, the bipolar pulse parameters are set per the maximum expected physiologic velocity. For monotonicity then, the product, TA_g, is selected such that $TA_g < \pi/(2\gamma V_{max})$. Accordingly, the phase-contrast image then presents relative flow information among vessels.

The phase of the RF excitation and reception is held constant throughout the acquisition. Both the phase-encoding and readout-dephasing lobes are applied just before readout to reduce both signal attenuation due to phase dispersion effects and flow misregistration artifacts.

Acquisition pulse sequence may be executed as either 2D projection or 3D volume acquisition. The 2D technique projects the excited slab onto a 2D image plane whose spatial orientation is selected prior to the study. The signal for overlapping vessels is vectorially added, and image intensity is determined by the amount of constructive or destructive interference. Thus, signal intensity at vessel crossings can be meaningless. Slabs of excitation as small as 3 mm may be obtained in the 2D method.

The advantage of the 2D technique is that an image, useful for localizing, can be produced in as little as 27 sec (NEX =

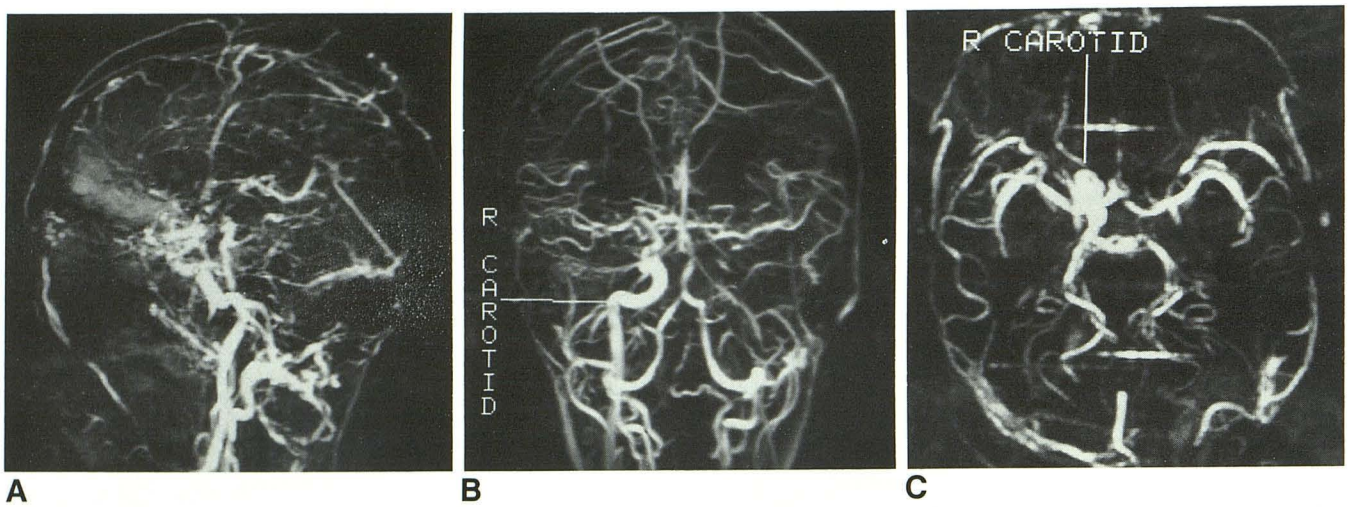

Fig. 8.—Superior sagittal sinus thrombosis.
***A*, Collapse image of subset of sagittal slices through superior sagittal sinus.**
***B*, Anteroposterior projection image of entire data set.**
***C*, Axial collapse image of region surrounding circle of Willis.**
Minimal or absent flow is noted in superior sagittal, transverse, and sigmoid sinuses along with jugular veins. No evidence of flow is seen in left internal carotid artery. These findings confirm clinical suspicion of thrombosis.

2) for three flow-encoded directions. Diagnostic-quality 2D projection angiograms can be obtained in about 5 min (NEX = 24 to span the cardiac period). These images can be used to localize a 3D acquisition, address clinical questions involving flow in major vessels, or achieve time resolution in a dynamic study. Disadvantages include the limitation of a single view angle per acquisition and decreased resolution from large elongated voxel shape because of the length of the project direction. 3D acquisition generally gave superior results when compared with 2D projection-mode acquisition for cerebral studies.

Saturation slabs can be used to decrease vascular complexity and to distinguish artery from vein in certain situations. For instance, in the neck, saturation of tissue superior to the excitation volume will tend to make venous blood lose signal while an inferior saturation will tend to make arterial blood lose signal.

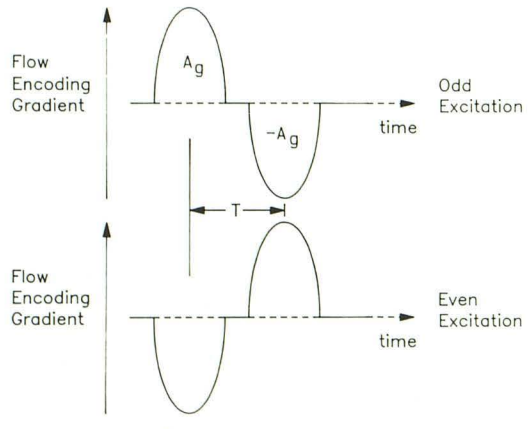

Fig. 9.—Bipolar flow-encoding gradient pulse. A spin with a velocity component parallel to flow-encoding gradient direction will undergo a phase shift. The bipolar pulse is applied on one gradient direction per acquisition sequence and is positioned as indicated in Fig. 1. T = time separation of the center of bipolar lobes; A_g = area under one lobe.

Phase Dispersion

The signal intensity of a voxel is also related to the phase dispersion within it. Phase dispersion arises from a range of velocities existing within an acquisition voxel, uncompensated orders of motion, and magnetic susceptibility variations. The greater the velocity dispersion, the greater the phase dispersion and, therefore, the lower the received signal. For laminar flow, the velocity profile across a vessel diameter is parabolic. For voxels at the center of a vessel with laminar flow, the velocity is greatest and dispersion is smallest, yielding a resultant signal that is largest. For voxels close to the wall, the velocity is smallest, dispersion greatest, and resultant signal smallest. Also, as the amount of flow encoding increases, the larger the amount of phase dispersion. Phase dispersion effects can become prominent at obstructions and at bends in vessels. Flow jets formed at obstructions may cause complex flow for some distance distal to the obstruction, as seen in Figures 7A and 7B. Within vessel curves, blood protons at the convexity of the bend are accelerated differently from those at the concavity. This induces helical and other complex flow patterns in the region. The loss of signal in the supraclinoid internal carotid artery is a good example of this phenomenon (Figs. 3B and 3C).

Signal from flow in a vessel may be attenuated when a vessel is near bone; for example, the vertebral arteries traversing the foramina of the cervical vertebrae or the carotid artery going through the petrous bone (Fig. 2). Calcium and cortical bone exhibit diamagnetic properties that cause magnetic field inhomogeneity in the surrounding region. Since

gradient refocusing does not counterbalance the effect of field inhomogeneity, signal may be attenuated and the localized segment of a blood vessel may appear diminished or missing.

The loss of signal owing to phase-dispersion effects can be lessened by using smaller voxels and shorter TEs. TEs can be reduced by pulse sequence refinements, higher root-mean-square power gradient amplifiers, and wider readout bandwidth.

Acquisition Time Issues

Currently, three sequential 3D acquisitions are required to encode for total flow. This incurs a 37-min acquisition time with the present pulse sequence implementation and instrument capabilities. Patient motion is clearly a potential problem. In our experience, however, patients generally cooperate in minimizing motion in the hope of avoiding contrast angiography. To date, only simple soft foam wedges have been placed aside the patient's head inside the head coil. A few examinations have failed owing to patient motion. Effort is being directed at producing a suitable head restraint. A prospective study is in progress that documents the compromised and failed examination rates.

To shorten the acquisition time, TR must be shortened and/or the number of excitations reduced. The means for reducing TR are the same as given for TE, as both will decrease concomitantly.

The number of excitations can be reduced by using fewer phase-encoding steps in one direction. The options here are decrease FOV or increase acquisition voxel size. Reducing the phase-encoding steps by one-half correspondingly halves the scan time. If a small voxel size is maintained, one direction of the FOV must be halved. Thin-section total-flow 3D angiograms having an acquisition matrix of 254 × 128 × 32 can be acquired in under 10 min.

Image Presentation

The wealth of visualized arteries and veins on the 3D image can make detection and study of disease difficult. Because data for MR angiograms are digital and obtained by 3D acquisition, there is great flexibility in image display. A projection image can be computed from any view angle by projecting the 3D image data into a 2D image. Various algorithms for assigning projection pixel (picture element of a 2D digital image) values are possible. The MR angiograms presented herein were computed by selecting the maximum voxel value along the projection ray path as the projection image pixel. When viewed statically spatial information is lost. Spatial perspective can be regained by displaying in cine format a series of these projection images computed from progressive view angles about an axis of rotation. The observer's ability to integrate information frame-to-frame allows complex spatial relationships of vessels to be perceived.

Simplified views are routinely used during interpretation. Collapse images, primary axis projection across selected subvolumes, bear a "tomogram effect" since overlying and irrelevant vessels are eliminated from the image. In many cases, 2D collapse images can very effectively reveal details of interest by presenting a simplified or unobstructed view and hence serve as the best representation. Viewing individual slices of the 3D flow image in the axial, sagittal, or coronal planes presents the finest details of the volume image.

Insight gained from our work suggests three important criteria are required for effective presentation of 3D flow images:

1. A consistent spatial perspective should be portrayed in the projection images. For example, a dim slow-flow vessel closer to the viewer should obscure a deeper, bright fast-flow vessel. Closer objects should be visualized as closer. Depth queuing should be consistent.
2. The relative flow information intrinsic to phase-contrast images should be presented correctly and consistently in the projection images.
3. Artifacts should not be introduced that jeopardize clinical efficacy.

The maximum-intensity projection algorithm violates objectives 1 and 2. No spatial perspective is supplied in the projection images other than the observer's inferences from frame-to-frame relative motions. At any given projection pixel location, a pixel is given the maximum flow signal regardless of context. Two vessels that cross always take on the higher flow value at their intersection regardless of which vessel is closer to the viewer. An anterior viewpoint is exactly equivalent to a posterior viewpoint. Also, as a projected volume is increased, small vessels and low-flow details tend to disappear. Vessel diameters tend to be undersized since signal from flow near vessel walls descends toward background levels. A representation algorithm satisfying these three objectives would markedly benefit 3D angiography interpretation.

Comparison with X-ray Contrast Angiography

Information obtained from contrast angiography and phase-contrast angiography differ. In contrast angiography, contrast material mixes with blood and attenuates an X-ray beam in order to produce a 2D image of vasculature. Laminar and complex flow cannot be directed distinguished. The morphology of the walls of a vessel is well visualized. In MR angiography, phase-dispersion effects along with slow peripheral velocities tend to cause low signal near vessel walls. Hence, the diameter of vessels will tend to appear smaller in MR phase-contrast angiography relative to contrast angiography. The velocity profile becomes much more complicated when the blood flow is pulsatile and/or the vessel cross section changes (e.g., bifurcates). In general, because flow-encoded signal near the vessel wall is low, morphologic characteristics of the wall including aneurysmal outpouching, ulcerations, and plaques may not be demonstrated as well by MR phase-contrast angiography. The inability of MR phase-contrast angiography to demonstrate the 2-mm internal carotid artery aneurysm shown on contrast angiography (Fig. 3) is probably related to low signal owing to voxel size, phase dispersion, and slow flow within the aneurysm.

The advantages of the phase-contrast technique when compared with contrast angiography include (1) noninvasive-

ness; (2) the ability to better manipulate data—especially when 3D acquisitions have been obtained and individual slices or subsets can be observed; (3) the potential to quantify flow; and (4) the ability to obtain total vascular information that may require two or more catheter placements in contrast angiography.

Phase-Sensitive vs Time-of-Flight (TOF) Methods

The two basic strategies that have emerged for 3D imaging of vasculature blood flow by MR are phase-contrast methods and TOF methods. Among the various TOF methods, clinical utility has been reported for the 2D sequential slice approach [7] and 3D volumetric method [8–10].

In TOF studies, influx of fully relaxed spins into the excited volume is used to advantage so that unsaturated inflowing blood will have detectably higher signal compared with stationary tissue in steady-state saturation. The differential saturation will depend on the T1 and T2 of tissue surrounding the vessels. Because flow is detected in a manner that is not dependent on flow-induced phase shifts, signal loss arising from pulsatile and complex flow is less problematic. Loss of signal from phase dispersion can be reduced with TOF since shorter TE is achievable and gradient waveforms compensating for velocity and acceleration are typically applied. Compared with phase-contrast techniques, this may allow better visualization of signal from complex flow. TOF methods, however, are limited since signal from slow and/or saturated flow cannot be separated from stationary tissue. More slowly flowing blood that has been subjected to many RF pulses will not have enough signal to be distinguished from surrounding tissues. Also, structures with a short T1, such as methemoglobin in a thrombus, may appear bright on TOF studies and, therefore, may be difficult to distinguish from flowing blood given the TOF angiogram alone.

The TOF image is sensitive to all velocity components of flow in a single acquisition. Consequently, complete flow information can be imaged in about 40% the time required by the phase-contrast technique (equal FOV, voxel size, and current implementations).

Advantages of phase contrast when compared with TOF generally include (1) detection of slow flow using small voxel size and, therefore, better definition of small vessels, vessel wall morphology, and normal and pathologic venous structures; (2) images that present relative flow information among vessels; (3) the potential for quantitative flow measurements; and (4) direct suppression of stationary tissue.

Conclusions

MR angiography provides the ability to directly image vasculature noninvasively. No single acquisition technique will likely serve in all clinical applications. Our experience in the head and neck suggests that MR phase-contrast angiography will achieve results comparable to IV digital subtraction angiography. Further work is required to shorten the acquisition time and concomitantly improve image quality, to define the relative roles of the various approaches to MR flow imaging, to refine and broaden clinical knowledge regarding MR angiograms, and to extend the technique to other body regions.

REFERENCES

1. Enge I, Edgren J, eds. *Patient safety and adverse events in contrast medium examinations.* International congress series #816. New York: Elsevier, **1989**
2. Dumoulin CL, Hart HR. Magnetic resonance angiography. *Radiology* **1986**;161:717–720
3. Dumoulin CL, Souza SP, Hart HR. Rapid scan magnetic resonance angiography. *Magn Reson Med* **1987**;5:238–245
4. Dumoulin CL, Souza SP, Walker MF, Wagle W. Three dimensional phase contrast angiography. *Magn Reson Med* **1989**;9:139–149
5. Walker MF, Souza SP, Dumoulin CL. Quantitative flow measurement in phase contrast MR angiography. *J. Comput Assist Tomogr* **1988**;12(2): 304–313
6. Rossnick S, Kennedy D, Laub G, et al. Three dimensional display of blood vessels in MRI (abstr). In: *Proc IEEE Computers in Cardiology Conference.* Piscataway, NJ: IEEE, **1986**:193–196
7. Keller PJ, Drayer BP, Fram EK, et al. MR angiography via 2D-acquisition but yielding a 3D-display: a work in progress. *Radiology* **1989**;173: 527–532
8. Masaryk TJ, Modic MT, Ross JS, et al. Intracranial circulation: preliminary clinical results with three-dimensional (volume) MR angiography. *Radiology* **1989**;171:793–799
9. Masaryk TJ, Modic MT, Ruggieri PM, et al. Three-dimensional (volume) gradient-echo imaging of the carotid bifurcation: preliminary clinical experience. *Radiology* **1989**;171:801–806
10. Dumoulin CL, Cline HE, Souza SP, Wagle WA, Walker MF. Three-dimensional time-of-flight magnetic resonance angiography using spin saturation. *Magn Reson Med* **1989**;11:35–46